

Kohn–Sham inversion with mathematical guarantees

Michael F. Herbst,^{1, 2,*} Vebjørn H. Bakkestuen,³ and Andre Laestadius^{3, 4, †}

¹*Mathematics for Materials Modelling (MatMat),
Institute of Mathematics & Institute of Materials,*

École Polytechnique Fédérale de Lausanne, 1015 Lausanne, Switzerland

²*National Centre for Computational Design and Discovery of Novel Materials (MARVEL),*

École Polytechnique Fédérale de Lausanne, 1015 Lausanne, Switzerland

³*Department of Computer Science, Oslo Metropolitan University, 0130 Oslo, Norway*

⁴*Hylleraas Centre for Quantum Molecular Sciences, Department of Chemistry,
University of Oslo, P.O. Box 1033 Blindern, N-0315 Oslo, Norway*

We use an exact Moreau–Yosida regularized formulation to obtain the exchange-correlation potential for periodic systems. We reveal a profound connection between rigorous mathematical principles and efficient numerical implementation, which marks the first computation of a Moreau–Yosida-based inversion for physical systems. We develop a mathematically rigorous inversion algorithm which is demonstrated for representative bulk materials, specifically bulk silicon, gallium arsenide, and potassium chloride. Our inversion algorithm allows the construction of rigorous error bounds that we are able to verify numerically. This unlocks a new pathway to analyze Kohn–Sham inversion methods, which we expect in turn to foster mathematical approaches for developing approximate functionals.

I. INTRODUCTION

Density-functional theory (DFT) simulations are an indispensable tool in chemistry, materials science and solid-state physics [1–3]. In this theory, the unknown is the electronic density $\rho(\mathbf{r})$ instead of the full many-body wavefunction, making computations substantially more tractable [4]. However, one of the key ingredients of DFT, the universal density functional, is not known explicitly [5]. One therefore usually employs the Kohn–Sham (KS) formulation [6], where all unknowns of DFT are collected into the exchange-correlation (xc) functional, which is subsequently approximated. Substantial work has been devoted to developing accurate xc functional approximations [7]. Although DFT is in principle exact, and despite significant advancements, KS-DFT still faces challenges in certain physical contexts. Notable difficulties include accurately describing processes involving fractional electronic charge, such as dissociation or charge-transfer excitations [8–10], as well as addressing the well-known band gap problem, where semiconductor band gaps are underestimated [11–15]. Developing better xc functional approximations thus remains a major research thrust [16]. One obstacle is a lack in mathematical understanding between the exact universal density functional and common approximations [3], making the rigorous construction of new and better functionals hard.

In this work we will focus on KS inversion [17–43], which has been suggested as a tool to aid the construction of xc functionals [36, 40, 42]. In 1994, van Leeuwen and Baerends [24] utilized an inversion scheme to improve approximations to the KS potential. More recently

there has been considerable interest in KS inversion, leading for example to targeted software packages such as *n2v* [44] and *KS-pies* [45]. Both implement a variety of established inversion schemes, beyond the van-Leeuwen–Baerends method including the Zhao–Morrison–Parr [22] (ZMP) and Wu–Yang [26] methods. While initial exploration of KS inversion has focused on isolated systems and molecules, recent works have begun to tackle a wide range of solid-state systems as well [43, 46]. In contrast to the standard KS formulation, where one is equipped with an approximate xc potential and determines the density from a variational principle (forward problem), KS inversion does the reverse: given a ground-state density one seeks the exact xc potential v_{xc} which reproduces the density in an auxiliary non-interacting setting. Unfortunately, KS inversion is far less studied than the forward KS-DFT problem. Additionally, the development of a robust and efficient numerical scheme for KS inversion remains an open challenge [40, 42, 44, 45, 47, 48].

In a recently established result [49], the xc potential has been obtained as a mathematical limit within the Moreau–Yosida (MY) regularized formulation of DFT [50–54]. This limit involves first finding the *proximal density* (of a ground-state density) and then utilizing the duality map between the density and potential spaces. This novel link is extremely promising as MY regularization deals with the non-differentiability of the exact universal functional [55]. Notably, for both the aforementioned fractional electronic charge as well as the band-gap problems, a profound connection to the non-differentiability of KS-DFT has been established in early works on DFT [11, 12].

Here, we focus on periodic systems, a setting that is particularly suited to obtain an efficient numerical scheme for KS inversion that maintains the connection to a rigorous mathematical formulation. Employing the Density-Functional ToolKit [56] (DFTK), we are able to

* michael.herbst@epfl.ch

† andre.laestadius@oslomet.no

propose an implementation, which is capable of performing KS inversion on systems of practical relevance, such as bulk silicon, potassium chloride, and gallium arsenide. Notably, in the context of realistic physical systems, this is the first time a MY-based framework has been applied for KS inversion. Being equipped with a MY inversion procedure within a strict mathematical framework, we demonstrate how this inversion scheme opens up new insights into convergence properties and error analysis. In particular, we develop first rigorous error bounds for inverse KS problems. This paves the way for improved numerical analyses of KS inversion and opens up novel opportunities for the development of density functionals.

The remainder of this article is structured as follows. In section II A, we briefly present the mathematical framework of the MY inversion scheme within a periodic setting. Furthermore, in section II B we relate the proximal density to the xc potential v_{xc} and present an error analysis that includes rigorous bounds based on the proximal mapping. Section III discusses our numerical implementation and results when applying the scheme to three bulk materials. Lastly, in section IV we give some concluding remarks.

II. MATHEMATICAL RESULTS

A. Background

Density-functional theory considers a system of N electrons subjected to a scalar potential $v(\mathbf{r})$ with the corresponding (lifted) operator $\hat{V} = \sum_{j=1}^N v(\mathbf{r}_j)$. We let \hat{T} and \hat{W} denote the kinetic energy and two-body interaction operators, respectively. Let $E^\lambda(v)$ denote the ground-state energy for the Hamiltonian $\hat{T} + \lambda\hat{W} + \hat{V}$ and $F^\lambda(\rho)$ the *exact* universal functional, where λ is the coupling constant. For our purposes, it will be enough to consider $\lambda = 0$ and $\lambda = 1$. We will use $\langle v, \rho \rangle$ to denote the dual pairing between $\rho \in \mathcal{D}$ and $v \in \mathcal{V} = \mathcal{D}^*$, where \mathcal{D} is a Banach space (complete normed space with norm $\|\cdot\|_{\mathcal{D}}$) and \mathcal{D}^* its dual (i.e., the space of bounded, linear functionals on \mathcal{D} with induced norm $\|\cdot\|_{\mathcal{V}}$). In the Levy formulation [57], we can compute a constrained-search universal functional \tilde{F}^λ from states that minimize all internal energy contributions (i.e., coming from $\hat{T} + \lambda\hat{W}$) under a density constraint. In addition, the Lieb functional is defined as

$$F^\lambda(\rho) = \sup_{v \in \mathcal{V}} \{E^\lambda(v) - \langle v, \rho \rangle\} \quad (1)$$

and will we take this formula as a definition of the universal functional in our setting. In general, $F^\lambda(\rho) \leq \tilde{F}^\lambda(\rho)$ and by construction F^λ is convex and lower semicontinuous. A set S is convex if the line segment $tx + (1-t)y \in S$ whenever $x, y \in S$. A functional defined on a convex set S is convex if for all $x, y \in S$ and $t \in (0, 1)$ we have $f(tx + (1-t)y) \leq tf(x) + (1-t)f(y)$. Moreover, f is

lower semicontinuous if $f(x) \leq \liminf_{y \rightarrow x} f(y)$ whenever $y \rightarrow x$.

Now, $F(\rho) := F^1(\rho)$ is the exact universal functional of fully interacting electrons. In addition, at $\lambda = 0$, $T(\rho) := F^0(\rho)$ is the kinetic-energy functional. Note that we follow the convention of omitting the superscript at $\lambda = 1$ and using T instead of the superscript $\lambda = 0$. This style also applies to both E and \tilde{F} . For our purposes, DFT can be viewed as an energy minimization problem: given an external potential v , find the corresponding density ρ such that $E(v) = F(\rho) + \langle v, \rho \rangle$. Employing a slightly different sign convention [58], E can be viewed as the Fenchel conjugate (or Legendre transform) of F , and F as the conjugate of E . The ground-state density is then found by the Hohenberg–Kohn *variational principle* [4]

$$E(v) = \inf_{\rho \in \mathcal{D}} \{F(\rho) + \langle v, \rho \rangle\}.$$

In particular, obtaining the ground-state density ρ is equivalent to saturating the Fenchel–Young inequality $E(v) \leq F(\rho) + \langle v, \rho \rangle$.

Next, we introduce the *Moreau–Yosida regularization* [59] of a density functional $\mathcal{F} : \mathcal{D} \rightarrow \mathbb{R}$ at $\rho_0 \in \mathcal{D}$ as the infimum of \mathcal{F} and a penalty term,

$$\mathcal{F}^\varepsilon(\rho_0) = \inf_{\rho \in \mathcal{D}} \left\{ \mathcal{F}(\rho) + \frac{1}{2\varepsilon} \|\rho - \rho_0\|_{\mathcal{D}}^2 \right\}, \quad (2)$$

where $\varepsilon > 0$ is the regularization parameter. We refer to Eq. (2) as an *infimal convolution*. Our further discussion will be limited to the case when \mathcal{F} is a convex and lower semicontinuous functional and \mathcal{D} a uniformly convex space (in fact a Hilbert space, but *not* identified with its dual). If $\mathcal{F} = F$ is the exact universal functional, then the (exact) ground-state energy, $E(v)$, of some external potential, v , can still be computed from F^ε using [51]

$$\begin{aligned} E^\varepsilon(v) &= \inf_{\rho \in \mathcal{D}} \{F^\varepsilon(\rho) + \langle v, \rho \rangle\}, \\ E(v) &= E^\varepsilon(v) + \frac{\varepsilon}{2} \|v\|_{\mathcal{V}}^2. \end{aligned}$$

The exact relation between $E(v)$ and $E^\varepsilon(v)$ follows from the fact that the MY regularization is an infimal convolution together with the underlying relation of Fenchel conjugate pairs. In this regard, regularizing F with the MY transform is *lossless* as far as the energy is concerned.

We consider systems which are periodic on a lattice with a unit cell denoted by $\Omega \subset \mathbb{R}^3$. The function spaces of interest are the periodic Sobolev spaces [60, Section 2] $H_{\text{per}}^s(\Omega, \mathbb{C})$, $s = \pm 1$, equipped with the norm

$$\|u\|_{H_{\text{per}}^s}^2 = \sum_{\mathbf{G}} (1 + |\mathbf{G}|^2)^s |\hat{u}_{\mathbf{G}}|^2, \quad (3)$$

where the sum is over the usual reciprocal lattice vectors \mathbf{G} . Henceforth, we assume that the densities ρ are elements of $\mathcal{D} = H_{\text{per}}^{-1}$ such that the potentials v are in $\mathcal{V} = H_{\text{per}}^1$. Denote by $J : \mathcal{D} \rightarrow \mathcal{V}$ the duality mapping, i.e., the canonical map from the primary space to its dual,

$$J(\rho) = \{v \in \mathcal{V} : \|v\|_{\mathcal{V}}^2 = \|\rho\|_{\mathcal{D}}^2 = \langle v, \rho \rangle\}. \quad (4)$$

By the definition of the duality mapping in Eq. (4) and together with the particular choices of vector spaces \mathcal{D} and \mathcal{V} (with their norms given by Eq. (3)), we obtain

$$J(\rho) = \sum_{\mathbf{G}} \frac{\hat{\rho}_{\mathbf{G}} e_{\mathbf{G}}}{1 + |\mathbf{G}|^2} \quad (5)$$

as the Fourier representation of $J(\rho)$. Here $\hat{\rho}_{\mathbf{G}}$ are the Fourier coefficients of ρ and $e_{\mathbf{G}}$ the associated (normalized) basis vectors. It thus follows from a direct calculation that

$$J[\rho](\mathbf{r}) = (\Phi * \rho)(\mathbf{r}) = \int_{\mathbb{R}^3} \frac{\rho(\mathbf{r}')}{4\pi |\mathbf{r} - \mathbf{r}'|} e^{-|\mathbf{r} - \mathbf{r}'|} d^3 r', \quad (6)$$

where $\Phi(\mathbf{r}) = \exp(-|\mathbf{r}|)/(4\pi|\mathbf{r}|)$ is the Yukawa potential. Thus, in the setting considered here, the duality mapping $J(\rho)$ is the convolution of the density ρ with the Yukawa potential, which will be of importance when calculating the MY regularization.

B. The Inversion Formula & Error Bounds

In the interest of an inversion algorithm, suppose we are given some accurate (and fixed) ground-state density ρ_{gs} for some periodic system of interacting particles. Moreover, assume that this density is non-interacting v -representable, i.e., there exist a potential for which ρ_{gs} is also a non-interacting ground-state density. In practice, ρ_{gs} could be obtained from various sources, e.g., experimental data, full configuration interaction [61], coupled-cluster [26], or quantum Monte-Carlo [18, 23, 46] calculations. The goal is then to obtain the one-body potential of the associated KS system, in which the aforementioned xc potential v_{xc} is the critical unknown.

Recall the *kinetic-only* functional $T(\rho)$ that was defined as the Legendre transform of the non-interacting ground-state energy $E^0(v)$, that is (with $\lambda = 0$ in Eq. (1))

$$T(\rho) = \sup_{v \in \mathcal{V}} \{E^0(v) - \langle v, \rho \rangle\}. \quad (7)$$

Then, together with the Hartree contribution $E_H(\rho)$ and the fixed external potential $v_{\text{ext}} \in \mathcal{V}$, the kinetic-only functional defines our convex and lower semicontinuous guiding density functional

$$\mathcal{F}(\rho) = T(\rho) + E_H(\rho) + \int_{\Omega} v_{\text{ext}} \rho. \quad (8)$$

As already remarked above, $T(\rho)$ is both convex and lower semicontinuous, whilst for $v_{\text{ext}} \in \mathcal{V}$, the linear (and therefore convex) map $\rho \mapsto \int_{\Omega} v_{\text{ext}} \rho$ is even continuous. Note that the periodic Coulomb potential, defined as the solution to the (periodic) Poisson equation with a uniform background charge, is in \mathcal{V} , which is also the case for the local potential term of typical pseudopotential approximations [62–64]. Next, since the periodic Hartree contribution $E_H(\rho) = \sum_{\mathbf{G} \neq 0} \frac{|\hat{\rho}_{\mathbf{G}}|^2}{|\mathbf{G}|^2}$ is convex it

remains to prove that it is lower semicontinuous. To that end, suppose that $\|\rho^n - \rho\|_{H_{\text{per}}^{-1}(\Omega)} \rightarrow 0$. Since strong convergence implies that the norms are convergent, we have $\|\rho^n\|_{H_{\text{per}}^{-1}} \rightarrow \|\rho\|_{H_{\text{per}}^{-1}}$. However, $E_H(\rho)$ can be bounded by $\|\rho\|_{H_{\text{per}}^{-1}}^2$ from both above and below using that $|\mathbf{G}|^2 \leq 1 + |\mathbf{G}|^2 \leq \text{constant} \times |\mathbf{G}|^2$ for $\mathbf{G} \neq 0$, i.e.,

$$C_1 \|\rho\|_{H_{\text{per}}^{-1}}^2 \leq E_H(\rho) \leq C_2 \|\rho\|_{H_{\text{per}}^{-1}}^2$$

for some constants $C_1, C_2 > 0$. This implies that $E_H(\rho)$ is a continuous function in the $H_{\text{per}}^{-1}(\Omega)$ topology, which directly implies lower semicontinuity.

From the above discussion, it is clear that our choice of \mathcal{F} (Eq. (8)) is convex and lower semicontinuous, and thus eligible to the Moreau–Yosida program outlined in section II A. The key optimization problem of our inversion scheme is the minimization over $\rho \in \mathcal{D}$ of

$$\mathcal{E}(\rho; \rho_{\text{gs}}) = \mathcal{F}(\rho) + \frac{1}{2\varepsilon} \|\rho - \rho_{\text{gs}}\|_{\mathcal{D}}^2. \quad (9)$$

The functional $\rho \mapsto \mathcal{E}(\rho; \rho_{\text{gs}})$ is strictly convex and lower semicontinuous on the Hilbert space \mathcal{D} and the minimum is attained at a unique point [59] $\rho_{\text{gs}}^{\varepsilon} = \text{argmin}_{\rho} \mathcal{E}(\rho; \rho_{\text{gs}})$, referred to as the proximal density of ρ_{gs} . In the limit $\varepsilon \rightarrow 0^+$, it holds from [59, Prop. 1.146] that $\rho_{\text{gs}}^{\varepsilon} \rightarrow \rho_{\text{gs}}$. Since $\partial \frac{1}{2} \|\rho\|_{\mathcal{D}}^2 = J(\rho)$, we have the stationary condition

$$\underline{\partial} \mathcal{F}(\rho_{\text{gs}}^{\varepsilon}) + \frac{1}{\varepsilon} J(\rho_{\text{gs}}^{\varepsilon} - \rho_{\text{gs}}) \ni 0$$

for the minimization of \mathcal{E} . Here $\underline{\partial} \mathcal{F}$ denotes the subdifferential of \mathcal{F} and is the collection of all tangent functionals of \mathcal{F} . Under the assumption that the zero element of \mathcal{V} belongs to the set $\underline{\partial} \mathcal{F}(\rho_{\text{gs}}) + v_{\text{xc}}$ for some v_{xc} (i.e., the assumption of non-interacting v -representability), we obtain v_{xc} as the limit of $v_{\text{xc}}^{\varepsilon} = \frac{1}{\varepsilon} J(\rho_{\text{gs}}^{\varepsilon} - \rho_{\text{gs}})$ as $\varepsilon \rightarrow 0^+$ by [49, Thm. 2]. For our choice of function spaces, this implies using Eq. (6) that

$$v_{\text{xc}}(\mathbf{r}) = \lim_{\varepsilon \rightarrow 0^+} \frac{1}{\varepsilon} \int_{\mathbb{R}^3} \frac{\rho_{\text{gs}}^{\varepsilon}(\mathbf{r}') - \rho_{\text{gs}}(\mathbf{r}')}{4\pi |\mathbf{r} - \mathbf{r}'|} e^{-|\mathbf{r} - \mathbf{r}'|} d^3 r'. \quad (10)$$

The proximal mapping $\rho \mapsto \rho^{\varepsilon}$ is a (firmly [65]) non-expansive operator. To demonstrate this, we slightly generalize the proof of [66, Prop. 2.3] to the case considered here, i.e., Hilbert spaces not identified with their duals. From the general fact that $-\frac{1}{\varepsilon} J(\rho^{\varepsilon} - \rho)$ is an element of $\underline{\partial} \mathcal{F}(\rho^{\varepsilon})$, it follows that

$$\varepsilon (\underline{\partial} \mathcal{F}^{\varepsilon}(\rho^{\varepsilon}) - \underline{\partial} \mathcal{F}^{\varepsilon}(\tilde{\rho}^{\varepsilon})) \ni J(\rho^{\varepsilon} - \tilde{\rho}^{\varepsilon}) - J(\tilde{\rho}^{\varepsilon} - \tilde{\rho}^{\varepsilon}).$$

Then by the linearity of J , we have

$$\varepsilon (\underline{\partial} \mathcal{F}^{\varepsilon}(\rho^{\varepsilon}) - \underline{\partial} \mathcal{F}^{\varepsilon}(\tilde{\rho}^{\varepsilon})) + J(\rho^{\varepsilon} - \tilde{\rho}^{\varepsilon}) \ni J(\rho^{\varepsilon} - \tilde{\rho}^{\varepsilon}).$$

Then taking the dual pairing with $\rho^{\varepsilon} - \tilde{\rho}^{\varepsilon}$ yields

$$\|\rho^{\varepsilon} - \tilde{\rho}^{\varepsilon}\|_{\mathcal{D}}^2 \leq \langle J(\rho^{\varepsilon} - \tilde{\rho}^{\varepsilon}), \rho^{\varepsilon} - \tilde{\rho}^{\varepsilon} \rangle, \quad (11)$$

where we have used the maximal monotonicity [67] of the subdifferential of \mathcal{F}^ε and that $\langle J(\rho), \rho \rangle = \|\rho\|_{\mathcal{D}}^2$. Using Hölder's inequality, we obtain

$$\|\rho^\varepsilon - \tilde{\rho}^\varepsilon\|_{\mathcal{D}} \leq \|\rho - \tilde{\rho}\|_{\mathcal{D}}, \quad (12)$$

which establishes the non-expansiveness of the proximal mapping. In fact, Eq. (11) proves the *firm* non-expansiveness [65].

Equation (12) gives an estimate at a fixed $\varepsilon > 0$ for the error when performing the inversion using a perturbed density $\tilde{\rho}_{\text{gs}} = \rho_{\text{gs}} + \Delta\rho$ rather than the exact reference ρ_{gs} . For the purpose of further investigations, let us define the ratio

$$Q_\varepsilon(\Delta\rho) := \frac{\|\rho_{\text{gs}}^\varepsilon - \tilde{\rho}_{\text{gs}}^\varepsilon\|_{\mathcal{D}}}{\|\Delta\rho\|_{\mathcal{D}}} \leq 1.$$

The ratio satisfies $Q_\varepsilon \rightarrow 1$ as $\varepsilon \rightarrow 0^+$, by the fact that $\rho^\varepsilon \rightarrow \rho$. The total error introduced in v_{xc} by using a $\tilde{\rho}_{\text{gs}}$ and terminating the inversion at an $\varepsilon > 0$ is by the triangle inequality

$$\|v_{\text{xc}} - \tilde{v}_{\text{xc}}^\varepsilon\|_{\mathcal{V}} \leq \|v_{\text{xc}} - v_{\text{xc}}^\varepsilon\|_{\mathcal{V}} + \|v_{\text{xc}}^\varepsilon - \tilde{v}_{\text{xc}}^\varepsilon\|_{\mathcal{V}}. \quad (13)$$

The first term is the error arising from terminating the inversion at $\varepsilon > 0$. This term is guaranteed to vanish as $\varepsilon \rightarrow 0^+$ by [49, Thm. 2] and will be negligible for sufficiently small ε , a behavior also seen in our numerical calculations. Of interest in this article is the second term in Eq. (13), i.e., the error arising from the use of an inexact density. In the literature, errors in the energy caused by the use of perturbed densities are referred to as *density-driven errors* [68–70]. We will therefore borrow the term “density-driven” when we speak of errors in the potentials caused by inexact densities. Using that $v_{\text{xc}}^\varepsilon = \frac{1}{\varepsilon} J(\rho_{\text{gs}}^\varepsilon - \rho_{\text{gs}})$ and similarly for $\tilde{v}_{\text{xc}}^\varepsilon$, the error bound,

$$\|v_{\text{xc}}^\varepsilon - \tilde{v}_{\text{xc}}^\varepsilon\|_{\mathcal{V}} \leq \frac{1 + Q_\varepsilon(\Delta\rho)}{\varepsilon} \|\Delta\rho\|_{\mathcal{D}}, \quad (14)$$

follows from the linearity of J , the triangle inequality, and Eq. (12). We remark that Eq. (14) is our main theoretical result and will be the focus of much of the numerical study in section III D. In particular, we will demonstrate numerically, that the ratio Q_ε — central to the above bound — is indeed confined to $0 \leq Q_\varepsilon \leq 1$ for physical systems of interest.

We next discuss the implementation of the presented inversion scheme as a practical inversion algorithm and verify the derived error bound, Eq. (14), for a few representative solid-state systems.

III. NUMERICAL RESULTS

A. Implementation of the Inversion Algorithm

In our inversion scheme the potential v_{xc} corresponding to the given density ρ_{gs} is obtained by taking the

$\varepsilon \rightarrow 0^+$ limit in Eq. (10). To numerically extrapolate this limit we simply employ an exponentially decreasing sequence in ε , ranging between 1 and about 10^{-7} and defer the investigation of a more tailored ε sequences to future work. For each ε we minimize Eq. (9) with respect to ρ as will be detailed below. This yields the proximal density $\rho_{\text{gs}}^\varepsilon$ from which we extract $v_{\text{xc}}^\varepsilon = \frac{1}{\varepsilon} J(\rho_{\text{gs}}^\varepsilon - \rho_{\text{gs}})$, i.e. by applying the duality mapping. As ε decreases, the expectation is that $v_{\text{xc}}^\varepsilon$ converges numerically to v_{xc} .

The uniqueness of the proximal density for a fixed $\varepsilon > 0$ implies that $\rho_{\text{gs}}^\varepsilon$ can be obtained from \mathcal{E} of Eq. (9) by any minimization procedure of choice. In agreement with the usual KS-DFT implementation for this setting we will employ a parametrization of the proximal density in terms of orthonormal orbitals $\Phi = (\psi_1, \dots, \psi_{N_b})$, i.e. $\int_{\Omega} \psi_i^* \psi_j = \delta_{ij}$. In this notation we do not make the k -points explicit, i.e. the sum over i runs over all orbitals at all reducible \mathbf{k} -points used to discretize the Brillouin zone. Moreover in this work we will only consider periodic insulators, such that we can avoid making spin explicit and simply take N_b to be the product of the number of electron pairs and the number of k -points. In this parametrization the density is thus obtained as

$$\rho_{\Phi}(\mathbf{r}) = 2 \sum_{i=1}^{N_b} |\psi_i(\mathbf{r})|^2$$

enabling to rewrite Eq. (9) as the minimization of

$$\begin{aligned} \mathcal{E}(\Phi, \rho_{\text{gs}}) = & \sum_{i=1}^{N_b} \int_{\Omega} |\nabla \psi_i|^2 + E_{\text{H}}(\rho_{\Phi}) \\ & + \int_{\Omega} v_{\text{ext}} \rho_{\Phi} + \frac{1}{2\varepsilon} \|\rho_{\Phi} - \rho_{\text{gs}}\|_{\mathcal{D}}^2 \end{aligned} \quad (15)$$

with respect to the orbitals Φ . Notice that in contrast to Eq. (9), for the numerical implementation we use the standard KS kinetic energy expression in terms of orbitals instead of the definition based on the Legendre transform discussed in Eq. (7).

Equation (15) has a similar structure to the usual energy expression in KS-DFT. The only difference is that the usual approximate xc functional is replaced by a penalty term $\frac{1}{2\varepsilon} \|\rho_{\Phi} - \rho_{\text{gs}}\|_{\mathcal{D}}^2$. As a result standard direct minimization techniques in KS-DFT [71–76] can be directly applied. Here, we minimize \mathcal{E} using a BFGS-based quasi-Newton scheme [77, 78] adapted to the geometrical structure (Stiefel manifold) due to orthogonality constraint between the orbitals. The optimization is stopped either if the optimizer has been obtained to machine precision or if the change in $\rho_{\text{gs}}^\varepsilon$ between two iterations drops below 0.01 ε . Here, this heuristic criterion yields a good compromise between the required computational time and the accuracy of $v_{\text{xc}}^\varepsilon$ as well as an excellent agreement with our theoretical error bounds as will be shown in Section III D. We defer an investigation of a more efficient stopping criterion to future work. Further details on the numerical procedure can be found on GitHub [79], where the source code to reproduce the numerical results and all figures are available.

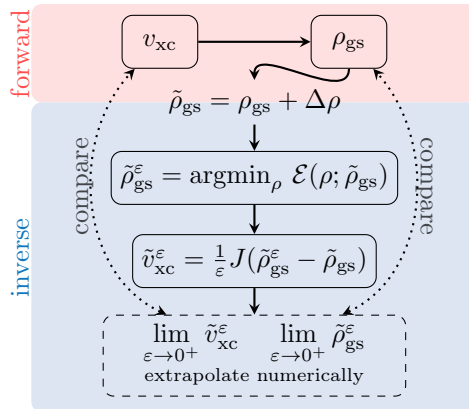


Figure 1. An illustration of the Moreau–Yosida (MY) inversion scheme. Given v_{xc} , a ground-state density ρ_{gs} is first computed in a forward, reference calculation. Here, $\Delta\rho$ represent an introduced error, resulting in an inexact reference density $\tilde{\rho}_{gs}$. For this $\tilde{\rho}_{gs}$, the proximal point $\tilde{\rho}_{gs}^\varepsilon$ is found from the MY regularization. An ε -dependent potential is then found by means of the duality mapping J , whereupon the potential is obtained by taking $\varepsilon \rightarrow 0^+$. The results of the inversion can then be compared with the forward scheme.

B. Computational Setup

For obtaining our numerical results we follow the procedure outlined in Fig. 1. We first perform a forward KS computation (red panel) yielding both an xc potential v_{xc} as well as a corresponding reference ground-state density ρ_{gs} . We employ the PBE xc functional [80] as well as the “standard” PBE pseudodojo pseudopotentials [64] with non-linear core corrections. Furthermore we use a k -point spacing of at most 0.12\AA^{-1} and a rather tight kinetic energy cutoff of about twice the value recommended for our selected pseudopotentials. This enables us to reliably study the effect of controlled perturbations $\Delta\rho$ to the reference density ρ_{gs} and test our error bounds (see Section III.D). Finally, the obtained density $\rho_{gs} + \Delta\rho$ is fed to the KS inversion procedure described in the previous Section III.B (Fig. 1, blue panel). We remark that in this step, to achieve consistency between the forward and inverse problem, the same pseudopotential approximation has been used. As a result an additional non-local potential term is added to Eq. (15) corresponding to the Kleiman–Bylander part of the pseudodojo pseudopotentials. For further details we refer to the reference implementation on GitHub [79].

We remark that this setup enables us to directly compare the extrapolated proximal density and the extrapolated xc potential to the respective quantities ρ_{gs} and v_{xc} obtained in the forward calculation. In the literature such a setup, where the same quantum-chemical model and discretization basis is employed for both the inversion and the forward calculation, is sometimes referred to as an *inverse crime* [32, 40, 81]. However, we remark that our main focus is to highlight the strict mathematical results offered by the MY inversion scheme. It is thus beneficial to be able to compare both density and poten-

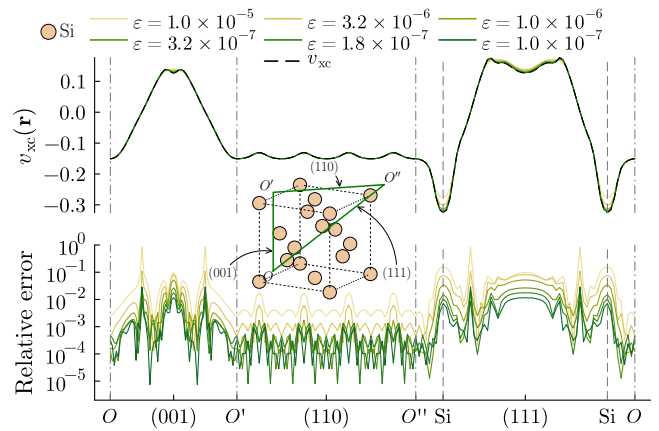


Figure 2. (top) Real-space plot of the reference xc potential along with the potential obtained from inversions for different values of the regularization parameter ε for bulk silicon. The potential is displayed along a closed path intersecting the high symmetry points [82, 83]. (bottom) The associated pointwise relative error of the potentials obtained from inversions at various ε compared to the reference xc potential. The crystalline structure and the path is shown in the inset.

tial from the inversion procedure against the reference from the forward scheme.

C. Exact inversion

First we consider the case of an “exact” inversion: we apply no additional noise ($\Delta\rho = 0$) and expect our inversion scheme to fully recover the xc potential. This setting we study on three bulk materials: silicon (Fig. 2) and gallium arsenide (Fig. 3) as well as potassium chloride (Fig. 4) as an example for an ionic solid.

Figure 2 shows the resulting potentials for bulk silicon, which are traced along the closed path in the unit cell suggested by Chen *et al.* [82, 83]. The top panel contrasts the reference v_{xc} against the potentials obtained from the inversion at selected values of ε . The bottom panel shows the pointwise absolute relative error of v_{xc}^ε against the reference v_{xc} . Two important features are observed. (1) Our inversion procedure accurately recovers the potential numerically: relative errors are below the 10 percentile for $\varepsilon \sim 10^{-6}$, and decrease by another order of magnitude by reducing ε by an order of magnitude. (2) Near the sharpest features of the potential, the pointwise convergence in ε is slower and the relative errors larger.

Figures 3 and 4 show the equivalent plots for gallium arsenide (GaAs) and potassium chloride (KCl) demonstrating the applicability to multiple standard material systems. The xc potential for GaAs is plotted along the same path as for silicon, starting between a Ga–Ga bond, while for KCl we start the trace directly on a potassium (K) atom, see respective insets. Contrasting with silicon, the absolute relative errors are slightly larger for GaAs and KCl at the same values of ε . Still, overall the reference potentials are accurately recovered (pointwise)

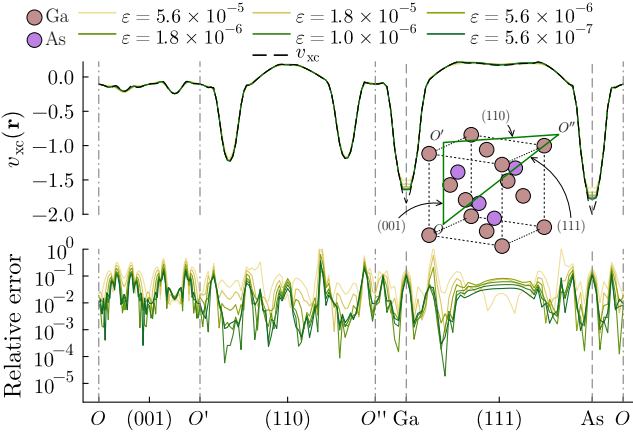


Figure 3. Analogous plots to Fig. 2 for gallium arsenide (GaAs) along the equivalent path shown in the inset crystalline structure.

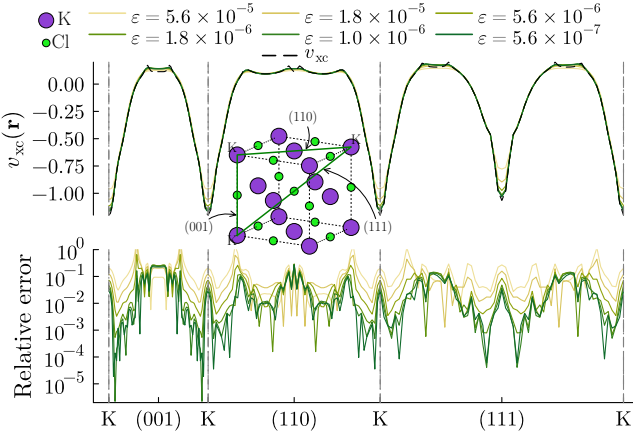


Figure 4. The equivalent plots to Figs. 2 and 3 for potassium chloride (KCl) displayed along a similar path shown in the inset crystalline structure.

across all three systems when no additional noise is applied ($\Delta = 0$).

D. Noisy inversion and error estimates

Having established the inversion algorithm to work well for multiple material systems in the absence of noise, we study numerically the susceptibility of the inversion algorithm to density-driven errors in the reference ground-state density, ρ_{gs} . Recall our notation $\tilde{\rho}_{\text{gs}} = \rho_{\text{gs}} + \Delta\rho$ for an inexact density. In practice, the erroneous part of the density, $\Delta\rho$, may arise from various sources depending on the origin of ρ_{gs} , e.g., basis truncations, change of basis, insufficiently converged reference densities, and experimental inaccuracies. Here, we limit ourselves to perturbations arising from an interpolation of the density utilizing a smaller plane-wave basis and focus solely on the bulk silicon test case.

Our numerical calculations show that such perturbations to the reference density do not alter the convergence

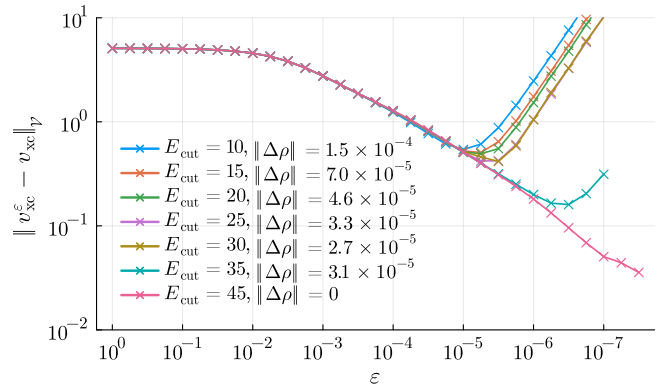


Figure 5. Convergence of v_{xc}^{ϵ} as a function of ϵ for various perturbations introduced by basis truncations for bulk silicon. E_{cut} determines the cut off in the Fourier basis and $\|\Delta\rho\|$ is the corresponding truncation error in the density in \mathcal{D} -norm. $E_{\text{cut}} = 45$ constitutes the (unperturbed) reference calculation.

properties of the potential as long as $\epsilon > \|\Delta\rho\|_{L^2_{\text{per}}}$, see Fig. 5. In particular, Fig. 5 shows the \mathcal{V} -norm difference of v_{xc}^{ϵ} and v_{xc} for various truncations, as indicated by the Fourier space cutoff (essentially zeroing out the components for which $|\mathbf{G}|^2 > 2E_{\text{cut}}$) and the associated norm of the perturbation, $\|\Delta\rho\|_{\mathcal{D}}$. For smaller ϵ the potential starts diverging from the reference in \mathcal{V} -norm.

In order to further study the errors arising in the inversion scheme, recall our main error bound (Eq. (14)),

$$\|v_{\text{xc}}^{\epsilon} - \tilde{v}_{\text{xc}}^{\epsilon}\|_{\mathcal{V}} \leq \frac{1 + Q_{\epsilon}(\Delta\rho)}{\epsilon} \|\Delta\rho\|_{\mathcal{D}}.$$

We note that the right-hand side can be universally bounded by $\frac{2}{\epsilon} \|\Delta\rho\|_{\mathcal{D}}$, i.e., the error in potential is small in the regime $\|\Delta\rho\|_{\mathcal{D}} \ll \epsilon$. To be able to further investigate Q_{ϵ} , we also note that by the construction of v_{xc}^{ϵ} (and $\tilde{v}_{\text{xc}}^{\epsilon}$) and the linearity of J , it follows that

$$\|v_{\text{xc}}^{\epsilon} - \tilde{v}_{\text{xc}}^{\epsilon} - \frac{1}{\epsilon} J(\Delta\rho)\|_{\mathcal{V}} \leq \frac{Q_{\epsilon}(\Delta\rho)}{\epsilon} \|\Delta\rho\|_{\mathcal{D}}. \quad (16)$$

Analogously to the ratio Q_{ϵ} , let us for Eqs. (14) and (16), respectively, define the ratios

$$R_{\epsilon}(\Delta\rho) := \epsilon \frac{\|v_{\text{xc}}^{\epsilon} - \tilde{v}_{\text{xc}}^{\epsilon}\|_{\mathcal{V}}}{\|\Delta\rho\|_{\mathcal{D}}},$$

$$S_{\epsilon}(\Delta\rho) := \epsilon \frac{\|v_{\text{xc}}^{\epsilon} - \tilde{v}_{\text{xc}}^{\epsilon} - \frac{1}{\epsilon} J(\Delta\rho)\|_{\mathcal{V}}}{\|\Delta\rho\|_{\mathcal{D}}}.$$

Using that $\|J(\Delta\rho)\|_{\mathcal{V}} / \|\Delta\rho\|_{\mathcal{D}} = 1$, the reverse triangle inequality applied to Eq. (16) gives $|R_{\epsilon} - 1| \leq Q_{\epsilon}$, i.e.,

$$0 \leq 1 - Q_{\epsilon}(\Delta\rho) \leq R_{\epsilon}(\Delta\rho) \leq 1 + Q_{\epsilon}(\Delta\rho) \leq 2. \quad (17)$$

Moreover, Eq. (16) implies that $0 \leq S_{\epsilon} \leq Q_{\epsilon} \leq 1$. Given the above, we remark that Q_{ϵ} is a central quantity in our error analysis.

By comparing the proximal densities of ρ_{gs} and that of $\tilde{\rho}_{\text{gs}}$, we can investigate the non-expansiveness of the proximal mapping by computing the ratio $Q_{\epsilon}(\Delta\rho)$. A

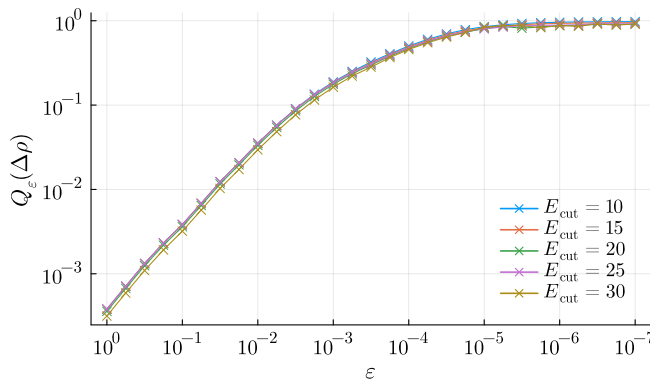


Figure 6. Related to the non-expansiveness of the proximal map, the ratio $Q_\varepsilon(\Delta\rho) = \|\rho_{\text{gs}}^\varepsilon - \tilde{\rho}_{\text{gs}}^\varepsilon\|_{\mathcal{D}} / \|\Delta\rho\|_{\mathcal{D}}$ is here shown for a decreasing sequence in ε . The corresponding values of $\|\Delta\rho\|$ are shown in Fig. 5. The plot demonstrates the convergence of $Q_\varepsilon \rightarrow 1$ as $\varepsilon \rightarrow 0^+$ numerically for bulk silicon.

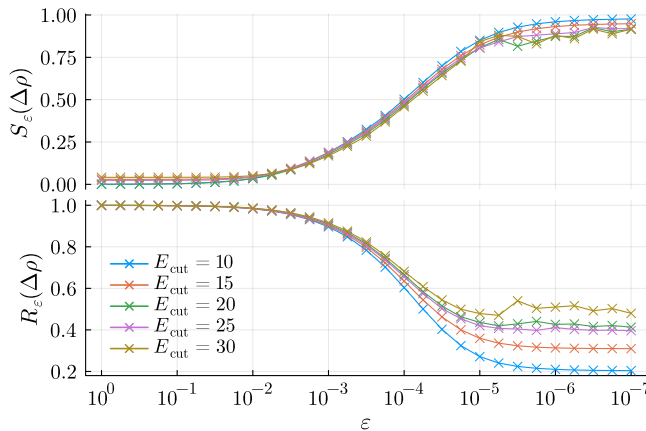


Figure 7. The ratios S_ε and R_ε as a function of ε for various basis truncations on bulk silicon, whose $\|\Delta\rho\|$ are given in Fig. 5. (top) S_ε , a mathematical equivalent measure to Q_ε , is small for large values of ε and increases to one as $\varepsilon \rightarrow 0$. (bottom) For large ε -values R_ε is similar to one, and approaches its lower bound (Eq. (17)) as $\varepsilon \rightarrow 0$. For $\varepsilon \lesssim 5 \times 10^{-6}$ the problem becomes numerically challenging, which manifests in small oscillations in the trends of both quantities.

plot of Q_ε is shown in Fig. 6 for a series of perturbations induced by truncations of the density in the Fourier basis, where the corresponding size of the perturbation $\|\Delta\rho\|_{\mathcal{D}}$ is shown in Fig. 5. By the proximal map, Q_ε is bounded to the range $[0, 1]$. From Fig. 6 we see that for large values of the regularization parameter ($\varepsilon \sim 1$) $Q_\varepsilon \ll 1$, and $Q_\varepsilon \rightarrow 1^-$ as $\varepsilon \rightarrow 0^+$. Additionally, we may obtain estimates for the error bounds on the xc potential, Eqs. (14) and (16), directly from the ratios R_ε and S_ε . In particular, Fig. 7 shows the ratios R_ε and S_ε (respectively bottom and top panels) obtained using the same $\tilde{\rho}_{\text{gs}}$ as in Fig. 6. Furthermore, Fig. 7 (top) shows that the ratio S_ε depend on ε in a very similar manner as Q_ε (see Fig. 6). Note that for large values of ε the ratio S_ε does not adhere exactly to the bound $S_\varepsilon \leq Q_\varepsilon$ (Eq. (16)), as can be seen by comparing Figs. 6 and 7. However, this is not surprising given that it is obtained from the difference of three quantities that should pointwise be almost

zero. For small values of ε , on the other hand, S_ε is in excellent agreement with the bound set by Q_ε , also satisfying $S_\varepsilon \rightarrow 1$ as $\varepsilon \rightarrow 0^+$. Moreover, Fig. 7 (bottom) shows that the ratio R_ε adheres strictly to the bound set by Q_ε (Eq. (14)). In particular, R_ε follow closely the lower bound $R_\varepsilon \geq 1 - Q_\varepsilon$ (Eq. (17)). Although obtaining the ratios involved in the error bounds, Eqs. (14), (16) and (17), is not computationally feasible in all practical calculations, our numerical results conform to the theoretical predictions. In fact, Figs. 6 and 7 even indicate that the ratio Q_ε may be estimated by a constant independent of $\Delta\rho$, but parametrically dependent on ε (and the guiding functional \mathcal{F}). Theoretically exploring this observation further marks a promising direction for future research towards more approximate bounds, which could be applied within a practical inversion scheme to make it more efficient and reliable. It is expected that improvements of the error bounds will enhance their applicability in practical calculations. Continued investigations will reveal if these first, but stringent, error estimates can be made useful in a broader sense.

IV. CONCLUSIONS

In this article we set the stage for further in-depth numerical analyses of KS inversion. Facing the challenges of numerically solving the many-body electronic-structure problem, progress is often the result from combining insights from mathematical analysis, more efficient numerical schemes as well as physically sound approximations. We have shown that the theoretical error bounds, Eqs. (14), (16) and (17), as well as the non-expansiveness, Eq. (12), are manifested in our numerical calculations. In our numerical study we targeted three bulk materials systems: two semiconductors (silicon and gallium arsenide) as well as an ionic salt (potassium chloride), demonstrating the applicability of our scheme to realistic systems. Since the calculations have been performed in a general DFT code with demonstrated performance on systems up to a few hundred electrons, a generalization to more involved systems is possible and inspired for. Future works should also aim to apply our presented inversion scheme to densities obtained from accurate sources other than forward KS algorithms. In this regard, considering reference densities from mean-field-like theories beyond semi-local DFT similar to recent work [43] represents a possible and interesting endeavour. In our numerical approach we follow the standard practice of plane-wave DFT to employ a pseudopotential for modelling the electron-nuclear interaction. While this approach is a practical necessity for efficient calculations, our current theoretical framework does not yet include the effects of non-local potentials. Closing this theoretical gap is an interesting direction for future research. We would also like to briefly comment on our choice of function spaces for the densities and potentials in our mathematical formulation. By choosing a potential space where the norm

also measures derivatives, we naturally penalize oscillations in the targeted xc potential. In addition, the choice of function space also dictates the form of the duality mapping, which in our setting leads to the numerically tractable form of a Yukawa kernel. Other options are of course possible and future investigations may reveal better choices.

The inversion scheme, the explicit form of v_{xc} (Eq. (10)), the use of the non-expansiveness of the proximal map, and the error bounds on the inverted potential are all novel theoretical results that are also numerically demonstrated. These results establish mathematical guarantees for KS inversion not previously seen, and also mark the first successful application of the MY framework to physical systems. We believe that such mathematical results, closely accompanied with numerical calculations, will significantly aid the development of more reliable KS inversion schemes. Moreover, the first stringent error bounds presented here open a new avenue for developing rigorous error estimates for density-potential inversion problems. Strengthened KS inversion schemes, in union with error analysis, should ultimately further the development of approximate density functionals. Furthermore, as highlighted by Shi and Wasserman [40], such enhanced understanding of

density-potential inversion may lead to advances in explorations of the Hohenberg–Kohn mapping, quantum embedding techniques, and enhanced optimised effective potentials.

Data Availability: Raw simulation data as well as source code to reproduce all numerical results and the plots presented in this article are openly available under DOI 10.5281/zenodo.14894064 or the GitHub repository [mfherbst/supporting-my-inversion](https://github.com/mfherbst/supporting-my-inversion) [79].

ACKNOWLEDGMENTS

AL and VHB were supported by the ERC-2021-STG grant agreement No. 101041487 REGAL. AL was also supported by the Research Council of Norway through CoE Hylleraas Centre for Quantum Molecular Sciences Grant No. 262695 and CCerror Grant No. 287906. MFH acknowledges support by the NCCR MARVEL, a National Centre of Competence in Research, funded by the Swiss National Science Foundation (Grant No. 205602). MFH and AL thank the Oberwolfach Research Institute for Mathematics where part of this research was conducted. We express our gratitude for fruitful discussions with Nicola Marzari and Markus Penz.

[1] K. Burke, Perspective on density functional theory, *J. Chem. Phys.* **136** (2012).

[2] P. Verma and D. G. Truhlar, Status and challenges of Density Functional Theory, *Trends in Chemistry* **2**, 302 (2020), special Issue - Laying Groundwork for the Future.

[3] A. M. Teale et al., DFT exchange: Sharing perspectives on the workhorse of quantum chemistry and materials science, *Phys. Chem. Chem. Phys.* **24**, 28700 (2022).

[4] P. Hohenberg and W. Kohn, Inhomogeneous electron gas, *Phys. Rev.* **136**, B864 (1964).

[5] N. Schuch and F. Verstraete, Computational complexity of interacting electrons and fundamental limitations of density functional theory, *Nature Physics* **5**, 732–735 (2009).

[6] W. Kohn and L. J. Sham, Self-consistent equations including exchange and correlation effects, *Phys. Rev.* **140**, A1133 (1965).

[7] J. Toulouse, Review of approximations for the exchange-correlation energy in density-functional theory, in *Density Functional Theory: Modeling, Mathematical Analysis, Computational Methods, and Applications*, edited by E. Cancès and G. Friesecke (Springer International Publishing, Cham, 2023) pp. 1–90.

[8] A. J. Cohen, P. Mori-Sánchez, and W. Yang, Insights into current limitations of Density Functional Theory, *Science* **321**, 792 (2008).

[9] D. G. Tempel, T. J. Martínez, and N. T. Maitra, Revisiting molecular dissociation in Density Functional Theory: A simple model, *J. Chem. Theory Comput.* **5**, 770 (2009).

[10] N. Helbig, I. V. Tokatly, and A. Rubio, Exact Kohn–Sham potential of strongly correlated finite systems, *J. Chem. Phys.* **131**, 224105 (2009).

[11] L. J. Sham and M. Schlüter, Density-functional theory of the energy gap, *Phys. Rev. Lett.* **51**, 1888 (1983).

[12] L. J. Sham and M. Schlüter, Density-functional theory of the band gap, *Phys. Rev. B* **32**, 3883 (1985).

[13] J. P. Perdew, R. G. Parr, M. Levy, and J. L. Balduz, Density-functional theory for fractional particle number: Derivative discontinuities of the energy, *Phys. Rev. Lett.* **49**, 1691 (1982).

[14] J. P. Perdew and M. Levy, Physical content of the exact Kohn–Sham orbital energies: Band gaps and derivative discontinuities, *Phys. Rev. Lett.* **51**, 1884 (1983).

[15] M. Grüning, A. Marini, and A. Rubio, Density functionals from many-body perturbation theory: The band gap for semiconductors and insulators, *J. Chem. Phys.* **124**, 154108 (2006).

[16] N. Mardirossian and M. Head-Gordon, Thirty years of density functional theory in computational chemistry: an overview and extensive assessment of 200 density functionals, *Molecular Physics* **115**, 2315 (2017).

[17] F. Aryasetiawan and M. J. Stott, Effective potentials in density-functional theory, *Phys. Rev. B* **38**, 2974 (1988).

[18] W. Knorr and R. W. Godby, Investigating exact density-functional theory of a model semiconductor, *Phys. Rev. Lett.* **68**, 639 (1992).

[19] A. Görling, Kohn–Sham potentials and wave functions from electron densities, *Phys. Rev. A* **46**, 3753 (1992).

[20] Q. Zhao and R. G. Parr, Constrained-search method to determine electronic wave functions from electronic densities, *J. Chem. Phys.* **98**, 543 (1993).

[21] Y. Wang and R. G. Parr, Construction of exact Kohn–

Sham orbitals from a given electron density, *Phys. Rev. A* **47**, R1591 (1993).

[22] Q. Zhao, R. C. Morrison, and R. G. Parr, From electron densities to Kohn–Sham kinetic energies, orbital energies, exchange-correlation potentials, and exchange-correlation energies, *Phys. Rev. A* **50**, 2138 (1994).

[23] W. Knorr and R. W. Godby, Quantum Monte Carlo study of density-functional theory for a semiconducting wire, *Phys. Rev. B* **50**, 1779 (1994).

[24] R. van Leeuwen and E. J. Baerends, Exchange-correlation potential with correct asymptotic behavior, *Phys. Rev. A* **49**, 2421 (1994).

[25] W. Yang and Q. Wu, Direct method for optimized effective potentials in Density-Functional Theory, *Phys. Rev. Lett.* **89**, 143002 (2002).

[26] Q. Wu and W. Yang, A direct optimization method for calculating density functionals and exchange–correlation potentials from electron densities, *J. Chem. Phys.* **118**, 2498 (2003).

[27] K. Peirs, D. Van Neck, and M. Waroquier, Algorithm to derive exact exchange-correlation potentials from correlated densities in atoms, *Phys. Rev. A* **67**, 012505 (2003).

[28] E. S. Kadantsev and M. J. Stott, Variational method for inverting the Kohn-Sham procedure, *Phys. Rev. A* **69**, 012502 (2004).

[29] F. A. Bulat, T. Heaton-Burgess, A. J. Cohen, and W. Yang, Optimized effective potentials from electron densities in finite basis sets, *J. Chem. Phys.* **127**, 174101 (2007).

[30] A. P. Gaiduk, I. G. Ryabinkin, and V. N. Staroverov, Removal of basis-set artifacts in Kohn–Sham potentials recovered from electron densities, *J. Chem. Theory Comput.* **9**, 3959 (2013).

[31] L. O. Wagner, T. E. Baker, E. M. Stoudenmire, K. Burke, and S. R. White, Kohn-Sham calculations with the exact functional, *Phys. Rev. B* **90**, 045109 (2014).

[32] D. S. Jensen and A. Wasserman, Numerical methods for the inverse problem of density functional theory, *Int J Quantum Chem.* **118** (2018).

[33] X. Zhang and E. A. Carter, Kohn-Sham potentials from electron densities using a matrix representation within finite atomic orbital basis sets, *J. Chem. Phys.* **148**, 034105 (2018).

[34] Q. Ou and E. A. Carter, Potential functional embedding theory with an improved Kohn–Sham inversion algorithm, *J. Chem. Theory Comput.* **14**, 5680 (2018).

[35] A. Kumar, R. Singh, and M. K. Harbola, Universal nature of different methods of obtaining the exact Kohn–Sham exchange-correlation potential for a given density, *J. Phys. B* **52**, 075007 (2019).

[36] B. Kanungo, P. M. Zimmerman, and V. Gavini, Exact exchange-correlation potentials from ground-state electron densities, *Nat Commun* **10**, 4497 (2019).

[37] A. Kumar and M. K. Harbola, A general penalty method for density-to-potential inversion, *Int J Quantum Chem.* **120**, e26400 (2020).

[38] R. Garrick, A. Natan, T. Gould, and L. Kronik, Exact generalized Kohn-Sham theory for hybrid functionals, *Phys. Rev. X* **10**, 021040 (2020).

[39] T. J. Callow, N. N. Lathiotakis, and N. I. Gidopoulos, Density-inversion method for the Kohn–Sham potential: Role of the screening density, *J. Chem. Phys.* **152**, 164114 (2020).

[40] Y. Shi and A. Wasserman, Inverse Kohn–Sham Density Functional Theory: Progress and challenges, *J. Phys. Chem. Lett.* **12**, 5308 (2021).

[41] J. Erhard, E. Trushin, and A. Görling, Numerically stable inversion approach to construct Kohn–Sham potentials for given electron densities within a Gaussian basis set framework, *J. Chem. Phys.* **156**, 204124 (2022).

[42] T. Gould, Toward routine Kohn–Sham inversion using the “Lieb-response” approach, *J. Chem. Phys.* **158**, 064102 (2023).

[43] V. Ravindran, N. I. Gidopoulos, and S. J. Clark, Local exchange-correlation potentials by density inversion in solids (2024), arXiv:2409.13647 [physics.chem-ph].

[44] Y. Shi, V. H. Chávez, and A. Wasserman, n2v: A density-to-potential inversion suite. a sandbox for creating, testing, and benchmarking density functional theory inversion methods, *WIREs Comput Mol Sci.* **12**, e1617 (2022).

[45] S. Nam, R. J. McCarty, H. Park, and E. Sim, KSpies: Kohn–Sham inversion toolkit, *J. Chem. Phys.* **154**, 124122 (2021).

[46] A. Aouina, M. Gatti, S. Chen, S. Zhang, and L. Reining, Accurate Kohn–Sham auxiliary system from the ground-state density of solids, *Phys. Rev. B* **107**, 195123 (2023).

[47] S. Crisostomo, R. Pederson, J. Kozlowski, B. Kalita, A. C. Cancio, K. Datchev, A. Wasserman, S. Song, and K. Burke, Seven useful questions in density functional theory, *Lett Math Phys* **113** (2023).

[48] J. Wrighton, A. Albavera-Mata, H. F. Rodríguez, T. S. Tan, A. C. Cancio, J. W. Dufty, and S. B. Trickey, Some problems in density functional theory, *Lett Math Phys* **113** (2023).

[49] M. Penz, M. A. Csirik, and A. Laestadius, Density-potential inversion from Moreau–Yosida regularization, *Electron. Struct.* **5**, 014009 (2023).

[50] S. Kvaal, U. Ekström, A. M. Teale, and T. Helgaker, Differentiable but exact formulation of density-functional theory, *J. Chem. Phys.* **140**, 18A518 (2014).

[51] A. Laestadius, M. Penz, E. I. Tellgren, M. Ruggenthaler, S. Kvaal, and T. Helgaker, Generalized Kohn–Sham iteration on Banach spaces, *J. Chem. Phys.* **149**, 164103 (2018).

[52] A. Laestadius, E. I. Tellgren, M. Penz, M. Ruggenthaler, S. Kvaal, and T. Helgaker, Kohn–Sham theory with paramagnetic currents: Compatibility and functional differentiability, *J. Chem. Theory Comput.* **15**, 4003 (2019).

[53] M. Penz, A. Laestadius, E. I. Tellgren, and M. Ruggenthaler, Guaranteed convergence of a regularized Kohn–Sham iteration in finite dimensions, *Phys. Rev. Lett.* **123**, 037401 (2019).

[54] M. Penz, A. Laestadius, E. I. Tellgren, M. Ruggenthaler, and P. E. Lammert, Erratum: Guaranteed convergence of a regularized Kohn–Sham iteration in finite dimensions [phys. rev. lett. 123, 037401 (2019)], *Phys. Rev. Lett.* **125**, 249902(E) (2020).

[55] P. E. Lammert, Differentiability of Lieb functional in electronic density functional theory, *Int. J. Quantum Chem.* **107**, 1943 (2007).

[56] M. F. Herbst, A. Levitt, and E. Cancès, DFTK: A Julian approach for simulating electrons in solids, *Proceedings of the JuliaCon Conference* **3**, 69 (2021).

[57] M. Levy, Universal variational functionals of electron densities, first-order density matrices, and natural spin-orbitals and solution of the v-representability problem, *Proc. Natl. Acad. Sci. USA* **76**, 6062 (1979).

[58] The reader familiar with the standard convex (Fenchel)

conjugate $f^*(y) = \sup_x (\langle y, x \rangle - f(x))$, can then compare to the DFT-adapted definitions $E(v) = F^\wedge(v) = -F^*(-v)$ and $F(\rho) = E^\vee(\rho) = (-E)^*(-\rho)$.

[59] V. Barbu and T. Precupanu, *Convexity and Optimization in Banach Spaces*, 4th ed., Springer Monographs in Mathematics (Springer Netherlands, 2012).

[60] E. Cancès, R. Chakir, and Y. Maday, Numerical analysis of the planewave discretization of some orbital-free and Kohn-Sham models, *ESAIM: Mathematical Modelling and Numerical Analysis* **46**, 341 (2012).

[61] S. Tribedi, D.-K. Dang, B. Kanungo, V. Gavini, and P. M. Zimmerman, Exchange correlation potentials from full configuration interaction in a Slater orbital basis, *J. Chem. Phys.* **159**, 054106 (2023).

[62] S. Goedecker, M. Teter, and J. Hutter, Separable dual-space Gaussian pseudopotentials, *Phys. Rev. B* **54**, 1703 (1996).

[63] C. Hartwigsen, S. Goedecker, and J. Hutter, Relativistic separable dual-space Gaussian pseudopotentials from H to Rn, *Phys. Rev. B* **58**, 3641 (1998).

[64] M. van Setten, M. Giantomassi, E. Bousquet, M. Verstraete, D. Hamann, X. Gonze, and G.-M. Rignanese, The pseudodojo: Training and grading a 85 element optimized norm-conserving pseudopotential table, *Computer Physics Communications* **226**, 39 (2018).

[65] We use the notion of a firmly non-expansive operator as in the case of a Hilbert space identified with its dual with the obvious inclusion of the duality mapping, i.e., Eq. (11).

[66] V. Barbu, *Nonlinear Differential Equations of Monotone Types in Banach Spaces*, 1st ed., Springer Monographs in Mathematics (Springer New York, 2010).

[67] A set $A \subset X \times X^*$ is said to be monotone if

$$\langle y_1 - y_2, x_1 - x_2 \rangle \geq 0 \quad \forall [x_i, y_i] \in A, i = 1, 2,$$

and maximally monotone if the set is not properly contained in any other monotone subset of $X \times X^*$ [66, Def. 2.1]. By the lower semicontinuity of the subdifferential of a convex functional, the maximal monotonicity follows.

[68] M.-C. Kim, E. Sim, and K. Burke, Understanding and reducing errors in Density Functional calculations, *Phys. Rev. Lett.* **111**, 073003 (2013).

[69] S. Nam, S. Song, E. Sim, and K. Burke, Measuring density-driven errors using Kohn-Sham inversion, *J. Chem. Theory Comput.* **16**, 5014–5023 (2020).

[70] A. D. Kaplan, C. Shahi, P. Bhetwal, R. K. Sah, and J. P. Perdew, Understanding density-driven errors for re-action barrier heights, *J. Chem. Theory Comput.* **19**, 532 (2023).

[71] M. C. Payne, M. P. Teter, D. C. Allan, T. A. Arias, and J. D. Joannopoulos, Iterative minimization techniques for ab initio total-energy calculations: molecular dynamics and conjugate gradients, *Rev. Mod. Phys.* **64**, 1045 (1992).

[72] G. Kresse and J. Furthmüller, Efficient iterative schemes for ab initio total-energy calculations using a plane-wave basis set, *Phys. Rev. B* **54**, 11169 (1996).

[73] X. Gonze, First-principles responses of solids to atomic displacements and homogeneous electric fields: Implementation of a conjugate-gradient algorithm, *Phys. Rev. B* **55**, 10337 (1997).

[74] A. A. Mostofi, P. D. Haynes, C.-K. Skylaris, and M. C. Payne, Preconditioned iterative minimization for linear-scaling electronic structure calculations, *J. Chem. Phys.* **119**, 8842 (2003).

[75] E. Vecharynski, C. Yang, and J. E. Pask, A projected preconditioned conjugate gradient algorithm for computing many extreme eigenpairs of a Hermitian matrix, *J. Comput. Phys.* **290**, 73 (2015).

[76] X. Dai, Z. Liu, L. Zhang, and A. Zhou, A conjugate gradient method for electronic structure calculations, *SIAM J. Sci. Comput.* **39**, A2702 (2017).

[77] A. Edelman, T. A. Arias, and S. T. Smith, The geometry of algorithms with orthogonality constraints, *SIAM J. Matrix Anal. Appl.* **20**, 303 (1998).

[78] N. Boumal, *Introduction to Optimization on Smooth Manifolds* (Cambridge University Press, 2023).

[79] github.com/mfherbst/supporting-my-inversion.

[80] J. P. Perdew, K. Burke, and M. Ernzerhof, Generalized gradient approximation made simple, *Phys. Rev. Lett.* **77**, 3865 (1996).

[81] D. S. Jensen, *Density-to-Potential Inversions in Density Functional Theory*, Ph.D. thesis, Purdue University (2016).

[82] S. Chen, M. Motta, F. Ma, and S. Zhang, Ab initio electronic density in solids by many-body plane-wave auxiliary-field quantum monte carlo calculations, *Phys. Rev. B* **103**, 075138 (2021).

[83] Starting from O , the high-symmetry middle point between the two silicon atoms of a unit cell, we follow along the route $O - (001) - O' - (110) - O'' - (111) - O$, where O' and O'' denote the nearest symmetry-equivalent points to O along the respective path (following [82]).